Hindawi
Geofluids
Volume 2022, Article ID 1900859, 13 pages
https://doi.org/10.1155/2022/1900859

Research Article

The Frequency Dependence of Poisson's Ratio in Fluid-Saturated Rocks

Liming Zhao,[1,2] **Tongjun Chen**,[1,2] **Xin Zhang**,[3] **and Tao Xing**[4]

[1]*Key Laboratory of Coalbed Methane Resources and Reservoir Formation Process of the Ministry of Education, China University of Mining and Technology, Xuzhou 221008, China*
[2]*School of Resources and Geosciences, China University of Mining and Technology, Xuzhou 221116, China*
[3]*Huayang New Material Technology Group Co., Ltd., Yangquan 045000, China*
[4]*Beijing Tan Chuang Resources Technology Co., Ltd., Beijing 100160, China*

Correspondence should be addressed to Tongjun Chen; tjchen@cumt.edu.cn

Received 10 June 2022; Accepted 11 August 2022; Published 31 August 2022

Academic Editor: Jin Qian

We investigated the frequency dependence of Poisson's ratio ν in partially/fully fluid-saturated rocks. Based on one dominant fluid flow mechanism at each condition, we theoretically summarized that (1) when a rock is partially saturated or transits from drained state to undrained state at full saturation, ν increases monotonously with frequency, and the associated attenuation $(1/Q_\nu)$ is positive with one peak. (2) When the rock transits from undrained state to unrelaxed state at full saturation, there are three cases: 1) ν increases monotonously with frequency and has positive $1/Q_\nu$ with one peak, 2) ν keeps constant with frequency and has no attenuation, 3) and ν decreases monotonously with frequency and has negative $1/Q_\nu$ with one peak. In this condition, the dependence is influenced by the concentrations of stiff and soft pores, the aspect ratio of soft pores, and the pore fluid bulk modulus. (3) When it comes to the transition from drained state to unrelaxed state at full saturation, ν can exhibit two shapes with frequency: 1) step shape with two positive attenuation peaks and 2) bell shape with one positive attenuation peak and one negative attenuation peak. Then, we conducted a numerical example to indicate the effect of influence factors (the concentrations of stiff and soft pores, the aspect ratio of soft pores, and the pore fluid bulk modulus) on Poisson's ratio from undrained state to unrelaxed state, and validated the theoretical analysis by the published experimental data. In addition, based on $1/Q_\nu$, we reanalyzed and validated the relationship between different attenuation modes (i.e., bulk attenuation $1/Q_K$, P-wave attenuation $1/Q_P$, extensional attenuation $1/Q_E$, and S-wave attenuation $1/Q_S$): (1) when $1/Q_\nu$ is positive, the relationship between them is $1/Q_K > 1/Q_P > 1/Q_E > 1/Q_S$; when $1/Q_\nu$ is 0, the relationship between them is $1/Q_K = 1/Q_P = 1/Q_E = 1/Q_S$; and when $1/Q_\nu$ is negative, the relationship between them is $1/Q_K < 1/Q_P < 1/Q_E < 1/Q_S$. The relationship between different attenuation modes does not depend on saturation state (partial or full saturation) or ν but on $1/Q_\nu$. This research provides the frequency dependence of Poisson's ratio in partially/fully saturated rocks, which helps better understand Poisson's ratio at different frequencies and saturation states and can be used to improve the accuracy of geophysical data interpretation, such as lithology identification, hydrocarbon characterization in conventional reservoir, and brittleness evaluation of shale/tight sandstones in unconventional reservoir.

1. Introduction

Poisson's ratio is a key constraint on the nature and composition of sedimentary rocks and plays an important role in geophysical exploration, such as identifying lithology, characterizing hydrocarbon in reservoir,and evaluating the brittleness of shale and tight sandstones [1–3]. When the sedimentary rocks are partially/fully fluid-saturated, similar to elastic moduli, Poisson's ratio can also be frequency-dependent, which significantly affects the accuracy of lithology identification, hydrocarbon characterization, and brittleness evaluation. Thus, it is essential to investigate the frequency dependence of Poisson's ratio in partially/fully fluid-saturated sedimentary rocks. However, scholars in

seismic rock physics commonly focus their attentions on the frequency dependence of elastic moduli and associated attenuations, such as Young's modulus and extensional attenuation, bulk modulus, and bulk attenuation [4–19]. When they experimentally investigate the frequency dependence of elastic moduli and associated attenuations, they measure Poisson's ratio together but take it as a bridge to obtain other elastic moduli under assumption that the rock is isotropic. Few works have been done to specifically focus on Poisson's ratio. Recently, Pimienta et al. [20] experimentally investigated the effect of fluids and frequencies on Poisson's ratio of fully fluid-saturated sandstone samples using dynamic stress-strain method. This brilliant work indicated the frequency dependence of Poisson's ratio for fully fluid-saturated rocks with a lot of soft pores (i.e., grain contacts and cracks) and revealed relevant internal physical mechanisms. They observed that Poisson's ratio of the sandstone sample exhibited frequency-dependent bell-shaped dispersion under water and glycerin saturation and correlated with two positive peaks in its attenuation (they called it phase shift). Then, they interpreted the observation with fluid flow mechanism at different scales and effective medium theory: The first attenuation peak is related to the transition from drained state to undrained state, which is caused by global fluid flow mechanism, and the second attenuation peak is related to the transition from undrained (relaxed) state to unrelaxed state, which is caused by squirt flow mechanism. Nevertheless, their work did not (1) investigate the frequency dependence of Poisson's ratio in rocks with a small number of soft pores, (2) examine the frequency dependence of Poisson's ratio attenuation, and (3) consider the frequency dependence of Poisson's ratio in partially fluid-saturated rocks.

To this end, we investigate the frequency dependence of Poisson's ratio and its attenuation in fluid-saturated rocks at both partial and full saturation states. With fluid flow mechanism at different scales, we first theoretically summarize the frequency dependence of Poisson's ratio and its attenuation when a rock is partially or fully fluid-saturated. Then, we conduct a numerical example to examine the factors influencing the frequency dependence of Poisson's ratio and its attenuation when the rock transits from undrained state to unrelaxed state. In next, we compare our theoretical analysis with published experimental data. Finally, with the help of Poisson's ratio attenuation, we discuss the relationships between different attenuation modes (i.e., bulk attenuation $1/Q_K$, P-wave attenuation $1/Q_P$, extensional attenuation $1/Q_E$, and S-wave attenuation $1/Q_S$) [21].

2. Theoretical Analysis

Poisson's ratio ν is defined as the negative of the ratio of transverse strain to the axial strain in an elastic medium when a uniaxial stress is applied [22]:

$$\nu = -\varepsilon_{\text{transverse}}/\varepsilon_{\text{axial}}, \tag{1}$$

where $\varepsilon_{\text{transverse}}$ is the transverse strain and $\varepsilon_{\text{axial}}$ is the axial strain.

Similar to the definition of elastic moduli's attenuations [21, 23], Poisson's ratio attenuation $1/Q_\nu$ here is defined as the ratio of the imaginary part of complex Poisson's ratio ν^* to the real part of complex Poisson's ratio ν^*:

$$\frac{1}{Q_\nu} = \frac{\text{Imag}(\nu^*)}{\text{Real}(\nu^*)}. \tag{2}$$

Under assumption that the medium is isotropic and linear elastic, Poisson's ratio ν can also be obtained by using bulk and shear moduli (K, μ) [24]:

$$\nu = \frac{3K/\mu - 2}{6K/\mu + 2}. \tag{3}$$

Taking the first-order derivative of ν with respect to K/μ (not shown here) indicates that ν increases monotonously with the increase of K/μ. Thus, we next theoretically investigate the frequency dependence of K/μ to obtain the frequency dependence of Poisson's ratio in partially/fully fluid-saturated isotropic rocks. And, in the following each condition, we assume that only one fluid flow mechanism plays dominant role in the frequency dependence of Poisson's ratio and its attenuation.

2.1. Partially Fluid-Saturated Condition. For partially fluid-saturated rock, when seismic wave passes through and mesoscopic fluid flow mechanism dominates, shear modulus keeps constant, while bulk modulus increases monotonously with frequency [18, 19, 25]. Thus, Poisson's ratio increases with frequency in the intermediate frequency range. Furthermore, from Kramers-Kronig relations (KKR) [26], the dispersion and attenuation are correlated for a linear viscoelastic medium; i.e., positive/negative dispersion corresponds to positive/negative attenuation. Poisson's ratio here has positive dispersion with increasing frequency, thus corresponding to positive Poisson's ratio attenuation. In addition, one positive attenuation peak appears [25, 27, 28].

2.2. Fully Fluid-Saturated Condition

2.2.1. Drained State to Undrained State. When fully fluid-saturated rock transits from drained state to undrained state and global fluid flow mechanism dominates, similar to the partially fluid-saturated condition, shear modulus keeps constant, while bulk modulus increases with frequency [15, 29–31]. The corresponding Poisson's ratio also increases monotonously with frequency, and its associated attenuation is positive with one peak [29, 30].

2.2.2. Undrained State to Unrelaxed State. When fully fluid-saturated rock transits from undrained state to unrelaxed state, squirt flow can occur, both the fluid-saturated bulk and shear moduli can increase with frequency, which depends on the type of pores in rock. There are three cases: (1) only stiff/round pores in rock, (2) only soft pores/cracks in rock, and (3) both stiff and soft pores in rock.

(1) Stiff/round Pores Only. When there are only stiff pores randomly distributed in the fully fluid-saturated rock, as

seismic wave passes through, there is no fluid pressure difference between different stiff pores, resulting in that no squirt flow occurs between different stiff pores [32, 33]. Thus, there is no dispersion in bulk and shear moduli for the fluid-saturated rock at different frequencies, so does the corresponding Poisson's ratio; i.e., Poisson's ratio has no frequency dependence from undrained state to unrelaxed state.

(2) Soft Pores/Cracks Only. When there are only soft pores randomly distributed in the fully fluid-saturated rock, as seismic wave passes through, bulk modulus has no/negligible dispersion under isotropic bulk stress, whereas shear modulus has an obvious dispersion under anisotropic shear stress [33, 34]. As a result, there is a monotonous decrease for Poisson's ratio when the frequency increases. Specially, the corresponding Poisson's ratio attenuation is negative based on KKR. Furthermore, one correlated negative attenuation peak is observed. The monotonous decrease depends on the aspect ratio and density of soft pores. With the aspect ratio of soft pores increasing to that of stiff pores, the decrease trend becomes smaller and disappears finally (Section 2.2.2 (1)).

(3) Stiff and Soft Pores. When the fully fluid-saturated rock contains both stiff and soft pores, the frequency dependence of Poisson's ratio becomes complex and has a monotonous decrease or increase trend or keeps constant (frequency-independent), which is related to the co-working of stiff and soft pores.

As shown in Section 2.2.2 (2), when there are only soft pores in rock, Poisson's ratio at undrained state is higher than the one at unrelaxed state. The frequency dependence of Poisson's ratio shows a monotonous decrease from undrained state to unrelaxed state. With stiff pores introduced, different fluid pressure exists between stiff and soft pores, and squirt flow occurs. Compared to the bulk and shear moduli at undrained state, squirt flow phenomenon dramatically increases the ones at unrelaxed state [4–6, 33, 35]. However, whether Poisson's ratio at unrelaxed state is larger than that at undrained state (i.e., whether the frequency dependence of Poisson's ratio has a monotonous increase) depends on the concentration of stiff and soft pores, the aspect ratio of soft pores, and the bulk modulus of pore fluid, which is investigated in the Numerical Modelling section.

2.2.3. Drained State to Unrelaxed State. Combining Sections 2.2.1 and 2.2.2, we can predict the frequency dependence of Poisson's ratio from drained state to unrelaxed state. The frequency dependence of Poisson's ratio has always monotonous increase from drained state to undrained state (Section 2.2.1). When Poisson's ratio also increases with frequency from undrained state to unrelaxed state (Section 2.2.2), the frequency dependence of Poisson's ratio from drained state to unrelaxed state exhibits step shape; i.e., Poisson's ratio first increases with frequency, then keeps almost constant with frequency, and finally increases again with frequency. Poisson's ratio attenuation is nonnegative with two positive attenuation peaks. On the other hand, when Poisson's ratio decreases with frequency from undrained state to unrelaxed state (Section 2.2.2), the frequency dependence of Poisson's ratio from drained state to unrelaxed state exhibits bell shape; i.e., Poisson's ratio first increases with frequency, then keeps almost constant with frequency, and finally decreases with frequency. Correspondingly, Poisson's ratio attenuation can be positive or negative with one positive attenuation peak and one negative attenuation peak.

3. Numerical Modelling

As the frequency dependence of Poisson's ratio in rock containing both stiff and soft pores from undrained state to unrelaxed state is more complex than that in other conditions, we conducted a numerical modelling example to investigate the effect of influence factors (i.e., the concentration of stiff and soft pores, the aspect ratio of soft pores, and the bulk modulus of pore fluid) on Poisson's ratio in this condition. Furthermore, as Poisson's ratio has monotonous frequency dependence, we mainly compared Poisson's ratio at undrained and unrelaxed states (i.e., low-frequency and high-frequency limits). We chose a simple effective medium model (crack-pore effective medium model, CPEM model, Appendix A) to indicate the effects. Qualitatively similar results hold for other models, such as differential effective medium (DEM) model. Then, we used Zener model (Appendix B) to show the frequency-dependent Poisson's ratio and its attenuation from undrained state to unrelaxed state [13, 15].

3.1. The Effect of Influence Factors. The CPEM model expresses drained/unrelaxed elastic moduli explicitly and is widely used in porous rocks with a small number of soft pores [33]. The undrained elastic moduli are then obtained using Gassmann's formula with the drained elastic moduli. The physical parameters in the modelling are listed in Table 1. As the CPEM model is valid at low soft pore density, we set the maximum value of soft pore density to be 0.5. For the fact that soft pore aspect ratio of 0.0001-~0.001 causes most of the attenuation and dispersion [36], we chose the aspect ratio to be 0.0005 and 0.005, respectively. We also chose two typical fluids (water and glycerin) as the pore fluid.

3.1.1. Stiff Pore Porosity. On the basis that a number of soft pores is randomly distributed in rock (the soft pore density here is kept at 0.5), with increasing stiff pore porosity, dry Poisson's ratio and Poisson's ratio at unrelaxed state increase gradually or almost keep constant, while Poisson's ratio at undrained state decreases rapidly (Figures 1(a) and 1(b)). It indicates that the introduction of stiff pores into rock has a more important influence on Poisson's ratio at undrained state (decreasing it). Furthermore, as stiff pore porosity increases, Poisson's ratio at unrelaxed state is first smaller than, then equal to, and finally larger than that at undrained state. When Poisson's ratio at unrelaxed state is smaller than that at undrained state, it corresponds that the frequency dependence of Poisson's ratio has a

Table 1: The physical parameters in the modelling.

Bulk modulus of mineral matrix K_0 (GPa)	37
Shear modulus of mineral matrix μ_0 (GPa)	44
Aspect ratio of soft pores α	0.0005/0.005
Soft pore density ρ	0-0.5
Stiff pore porosity ϕ_s	0-0.1
Bulk modulus of pore fluid K_f (GPa)	2.2(water)/4.4(glycerin)
Viscosity of pore fluid η (Pa•s)	0.001(water)/1(glycerin)

monotonous decrease from undrained state to unrelaxed state. On the other hand, when Poisson's ratio at unrelaxed state is larger than that at undrained state, it corresponds that the frequency dependence of Poisson's ratio has a monotonous increase from undrained state to unrelaxed state.

3.1.2. Soft Pore Density/Soft Pore Porosity. With increasing soft pores in rock (the stiff pore porosity is kept at 0.04 and 0.1, respectively), dry Poisson's ratio decreases, while both Poisson's ratio at undrained and unrelaxed states increases, and Poisson's ratio at undrained state changes faster than that at unrelaxed state (Figures 1(c)–1(f)). The Poisson's ratio difference at undrained and unrelaxed states indicates that the introduction of soft pores into rock also has a more important influence on Poisson's ratio at undrained state (increasing it). Besides, as soft pore density increases, Poisson's ratio at unrelaxed state can be always larger than that at undrained state (Figures 1(e) and 1(f)), corresponding to a monotonous increase of Poisson's ratio. Or, Poisson's ratio at unrelaxed state is first larger than, then equal to, and finally smaller than that at undrained state (Figures 1(c) and 1(d)), corresponding to different frequency dependence of Poisson's ratio.

3.1.3. Aspect Ratio of Soft Pores. When the soft pore density keeps constant (i.e., 0.5), the larger the aspect ratio of soft pores, the larger the stiff pore porosity where Poisson's ratio at undrained and unrelaxed states is equal with each other (Figures 1(a) and 1(b)). On the other hand, when the stiff pore porosity keeps constant (i.e., 0.04), the larger the aspect ratio of soft pores, the smaller the soft pore density where Poisson's ratio at undrained and unrelaxed states is equal with each other (Figures 1(c) and 1(d)).

3.1.4. The Bulk Modulus of Pore Fluid. Similar to the effect of aspect ratio of soft pores, when the soft pore density keeps constant (i.e., 0.5), the larger the bulk modulus of pore fluid, the larger the stiff pore porosity where Poisson's ratio at undrained and unrelaxed states is equal with each other (Figures 1(a) and 1(b)). When the stiff pore porosity keeps constant (i.e., 0.04), the larger the bulk modulus of pore fluid, the smaller the soft pore density where Poisson's ratio at undrained and unrelaxed states is equal with each other (Figures 1(c) and 1(d)).

3.2. Frequency-Dependent Poisson's Ratio and Its Attenuation. With the viscoelastic Zener model, we extend the glycerin-saturated Poisson's ratio in Figure 1(b) at stiff pore porosities 0.04 and 0.1 to show the frequency dependence of Poisson's ratio and its attenuation from undrained state to unrelaxed state (Figure 2). At stiff pore porosity of 0.04 (the aspect ratio of soft pores is 0.005 and the soft pore density is kept at 0.5), as Poisson's ratio at unrelaxed state is smaller than that at undrained state (Figure 1(b)), Poisson's ratio decreases monotonously with frequency (Figure 2(a)), and it corresponds to negative attenuation and one negative attenuation peak (Figure 2(b)). On the other hand, at stiff pore porosity of 0.1, Poisson's ratio at unrelaxed state is larger than that at undrained state (Figure 1(b)), and Poisson's ratio thus increases monotonously with frequency (Figure 2(a)), corresponding to positive attenuation and one positive attenuation peak (Figure 2(b)).

4. Theoretical Analysis Validation with Published Experimental Data

Frequency-dependent Poisson's ratio data sets have been reported for different saturation states and different types of reservoir rocks (limestones, sandstones, and tight sandstones) in a wide frequency range using dynamic stress-strain method, mostly being a bridge to calculate other elastic moduli and their attenuations. Here, we presented the data sets to validate the previous theoretical analysis. We also used KKR [26] to verify the published Poisson's ratio data sets.

4.1. Partially Fluid-Saturated Condition. Sun et al. [18] quantitatively assessed the dispersion and associated attenuation of elastic properties in partially water-saturated Indiana limestone sample (from 0.004 to 100 Hz). They obtained partial saturation by two methods: drying and imbibition. For high saturations from drainage method (>80%, i.e., 87%, 89%, 92%, and 99%), Poisson's ratio is frequency-dependent and has obvious dispersion and one clear attenuation peak. Furthermore, the corresponding shear modulus shows almost constant with frequency, saturations and fluid distribution. With a new developed numerical model, which takes the fluid distribution obtained from CT as input, they attributed the observed elastic moduli's dispersion and attenuation to mesoscopic fluid flow. We present the frequency-dependent Poisson's ratio and its associated attenuation at the saturation degree of 89%. In Figure 3, Poisson's ratio increases with frequency, while Poisson's ratio attenuation keeps positive with one obvious peak, corresponding to Section 2.1. The measured Poisson's ratio shows good agreement with the one calculated

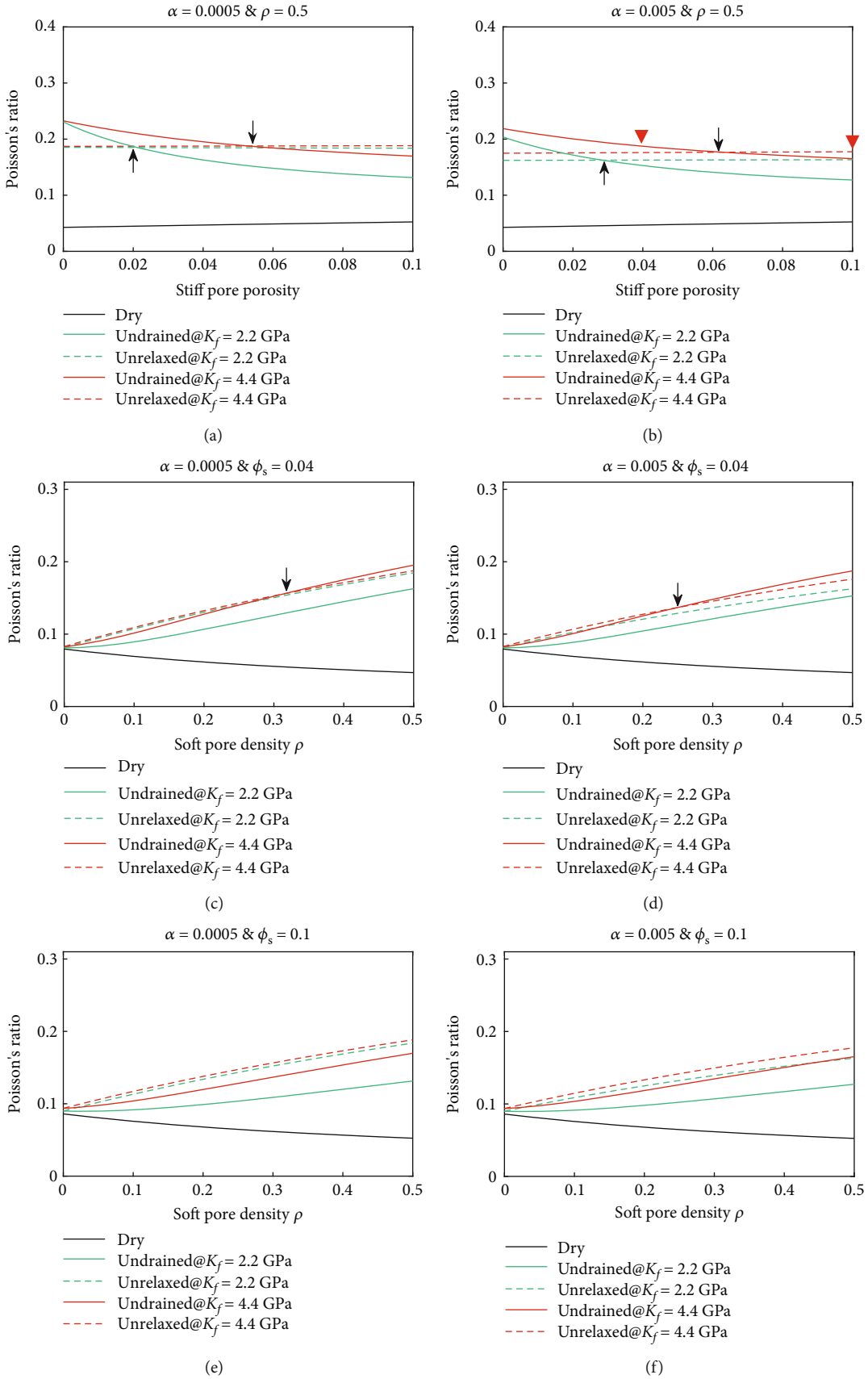

Figure 1: Modelling the effect of influence factors (i.e., the concentration of stiff and soft pores, the aspect ratio of soft pores, and the pore fluid bulk modulus) on Poisson's ratio with the CPEM model.

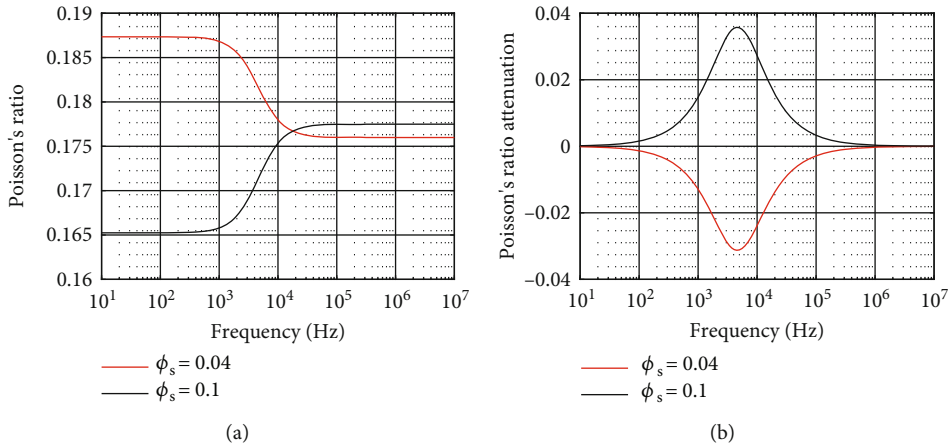

Figure 2: Modelling the frequency-dependent Poisson's ratio and its attenuation from undrained state to unrelaxed state with the viscoelastic Zener model.

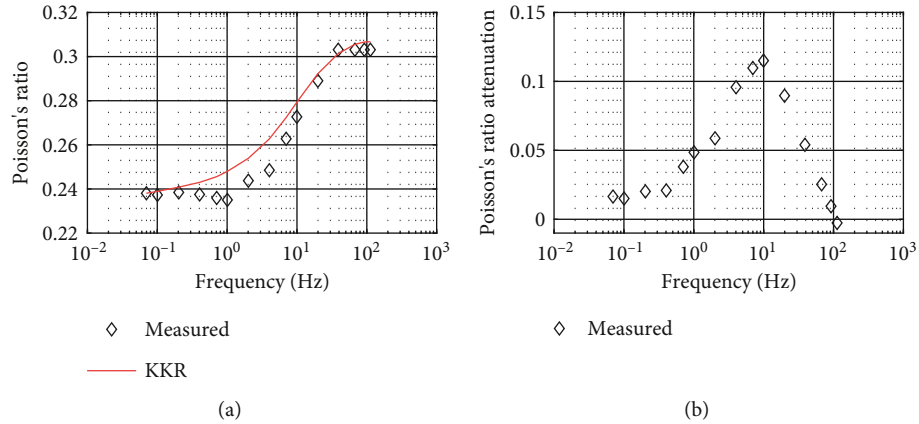

Figure 3: The frequency dependence of Poisson's ratio and it associated attenuation of partially water-saturated Indiana limestone sample (from Sun et al. [18]).

by KKR (data from other saturation degrees are also consistent with KKR well, but not shown here).

4.2. Fully Fluid-Saturated Condition: Drained State to Undrained State. Borgomano et al. [15] measured the dispersion and attenuation of elastic moduli and Poisson's ratio of a Lavoux limestone sample in the frequency range of 0.001-10 Hz. A dispersion appears at ~0.2 Hz for the glycerin-saturated condition, affecting all the elastic moduli and Poisson's ratio except the shear modulus. Based on 1-D poroelastic model [29], they concluded that the dispersion is related to the drained/undrained transition. In Figure 4, We present the frequency-dependent Poisson's ratio and its associated attenuation for the glycerin-saturated Lavoux limestone sample. Poisson's ratio has a monotonous increase as the frequency increases, and the attenuation is positive with one peak, validating the theoretical analysis in Section 2.2.1. The measured Poisson's ratio shows reasonable consistence with the one calculated by KKR.

4.3. Fully Fluid-Saturated Condition: Undrained State to Unrelaxed State. Sun et al. [17] investigated the impact of microstructure heterogeneity and local measurements on the dispersion and attenuation of elastic moduli of fully saturated sandstone rock. Using dynamic stress-strain method and two pairs of strain gauges at different locations, they observed the same global flow but different squirt flow at frequencies 1-300 Hz. Although the different squirt flow induces different magnitudes of the dispersion and attenuation of elastic moduli and Poisson's ratio, both of them indicate the transition from undrained state to unrelaxed state for the fluid-saturated rock. We chose one data set to show the frequency dependence of Poisson's ratio and its attenuation from undrained state to unrelaxed state (oil-saturated, pair #1 in their paper). For the oil-saturated sandstone sample, the stiff pore porosity is ~22%, the aspect ratio of soft pore is 0.00045, and the soft pore density is ~0.11. In Figure 5, the squirt-flow-related Poisson's ratio increases with frequency, and the attenuation has positive values with one peak, corresponding to Section 2.2.2. The predictions of KKR deviate slightly from the measured Poisson's ratio; however, the trend fits the measured data relatively well. Considering that the measurement errors of Poisson's ratio and its attenuation are ±0.006 and ±0.008, respectively

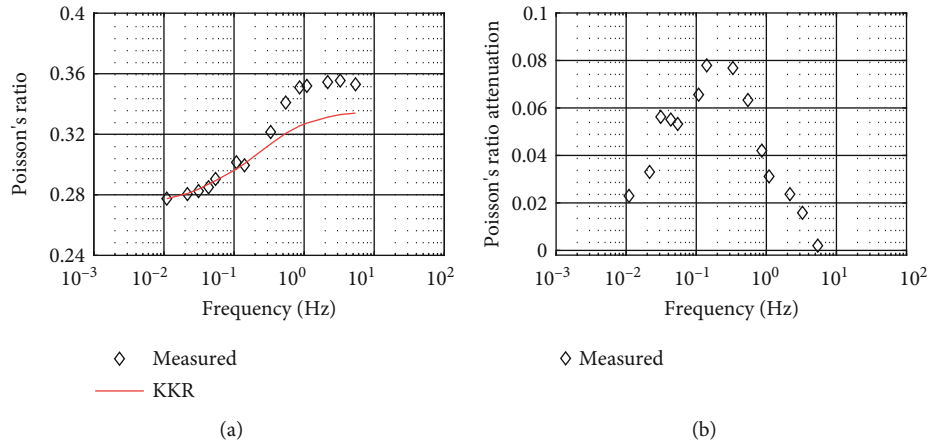

Figure 4: The frequency dependence of Poisson's ratio and it associated attenuation of the glycerin-saturated Lavoux limestone sample (from Borgomano et al. [15]).

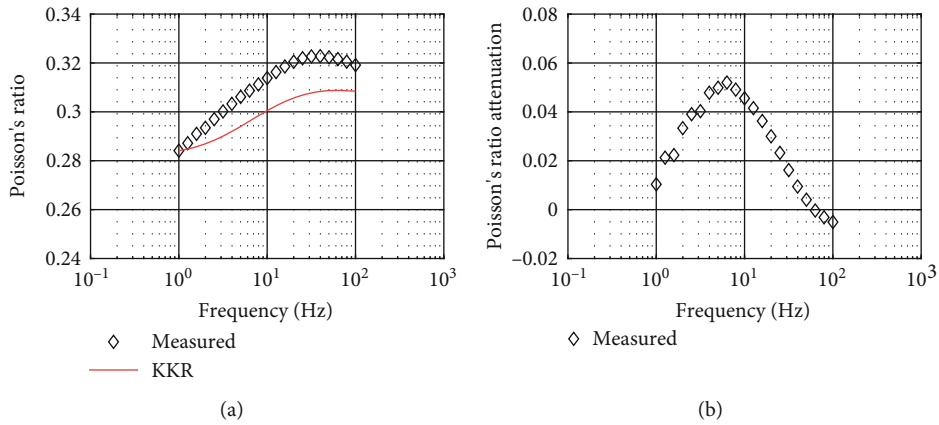

Figure 5: The frequency dependence of Poisson's ratio and it associated attenuation of oil-saturated sandstone sample (from Sun et al. [17]).

[17], the KKR calculation is reasonably consistent with the measured Poisson's ratio. Furthermore, the frequency dependence of Poisson's ratio agrees well with that in Figures 1(c) and 1(e) the Numerical Modelling section (i.e., rock contains large stiff pore porosity and small soft pore density).

On the other hand, Pimienta et al. [20] conducted low-frequency experiments (0.005-100 Hz) on Fontainebleau sandstone samples to explore the effect of fluids and frequencies on Poisson's ratio. When one sandstone sample is fully saturated with glycerin, the frequency dependence of Poisson's ratio and its attenuation at frequencies 0.1-100 Hz is mainly caused by squirt flow, corresponding to the transition from undrained state to unrelaxed state. Figures 6(a) and 6(b) show the measured data at effective pressure of 1 MPa (sample Fo7 in their paper) and the calculated KKR. The total porosity of the sample is ~7.3%, the aspect ratio of soft pores is ~0.001 or slightly lower, and the soft pore density is ~1. Poisson's ratio decreases monotonously with frequency; however, Poisson's ratio attenuation has positive values. The KKR calculation is not in agreement with the measured data, inferring that the monotonous decrease of Poisson's ratio should correspond to negative Poisson's ratio attenuation. When we revised Poisson's ratio attenuation to negative values (Figure 6(d)), the new KKR prediction agrees well with the measured one (Figure 6(c)), validating the theoretical analysis in Section 2.2.2.

4.4. Fully Fluid-Saturated Condition: Drained State to Unrelaxed State. Here, we also present the experimental data from Sun et al. [17] and Pimienta et al. [20] to indicate the frequency dependence of Poisson's ratio from drained state to unrelaxed state (Figure 7). For the sandstone sample with large stiff pore porosity and small soft pore density (Figures 7(a) and 7(b)), the transition from drained state to unrelaxed state exhibits "step" shape, and there are two positive attenuation peaks corresponding to the drained/undrained transition and the undrained/unrelaxed transition, respectively. On the other hand, for the sandstone sample with small stiff pore porosity and large soft pore density (Figures 7(c) and 7(d)), the transition from drained state to

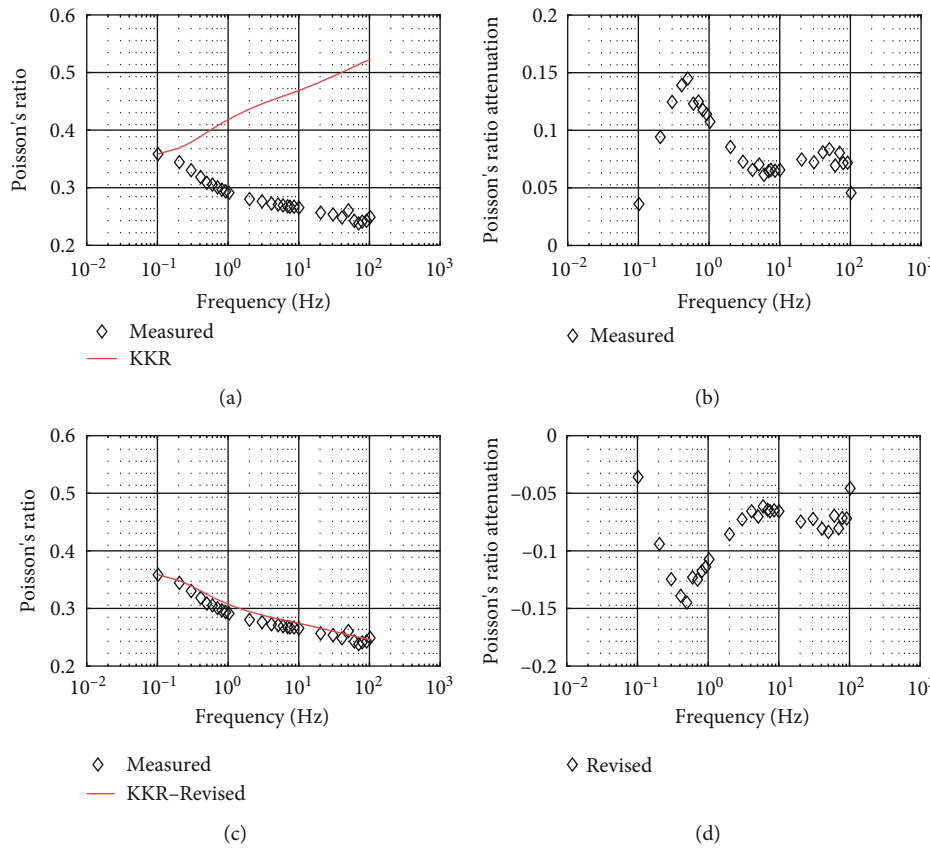

Figure 6: The frequency dependence of Poisson's ratio and it associated attenuation of the glycerin-saturated Fontainebleau sandstone sample (from Pimienta et al. [20]).

unrelaxed state exhibits "bell" shape, and there are one positive attenuation peak and one negative attenuation peak. The positive attenuation peak corresponds to the drained/undrained transition, whereas the negative attenuation peak corresponds to the undrained/unrelaxed transition. When the frequency dependence of Poisson's ratio exhibits "step" shape, all of Poisson's ratio attenuation is nonnegative, and the negative values can be attributed to the measurement error [17] (Figure 7(b)). The KKR calculation shows reasonable consistency with the measured Poisson's ratio (Figure 7(a)). On the contrary, when the frequency dependence of Poisson's ratio exhibits "bell" shape, Poisson's ratio attenuation related to the undrained/unrelaxed transition should be negative (Figure 7(d)). With the revised Poisson's ratio attenuation, the corresponding KKR calculation is in good agreement with the measured Poisson's ratio (Figure 7(c)).

5. Discussion

5.1. The Negative Poisson's Ratio Attenuation from Undrained State to Unrelaxed State. In the Theoretical Analysis section, Poisson's ratio attenuation $1/Q_\nu$ is defined as the ratio between the imaginary and real parts of complex Poisson's ratio ν^*. With this definition, Poisson's ratio attenuation can be obtained by $\tan(\varphi_1 - \varphi_2)$, where $(\varphi_1 - \varphi_2)$ is the phase of complex Poisson's ratio ν^*, φ_1 is corresponding to the phase of the transverse strain, and φ_2 is corresponding to the phase of the axial strain [20, 37, 38]. When it comes to the transition from undrained state to unrelaxed state, as the frequency increases, squirt flow effect decreases both the transverse and axial strains, which Poisson's ratio depends on. Poisson's ratio cannot always increase with frequency, which is influenced by the relative variation between the decreasing transverse and axial strains. Meanwhile, the phase of the transverse strain (φ_1) can lag behind to that of the axial strain (φ_2), thus resulting in the negative Poisson's ratio attenuation. On the contrary, when calculating the elastic moduli's attenuations with $\tan(\varphi_1 - \varphi_2)$, φ_1 is the phase of the applied stress, and φ_2 is the phase of the corresponding strain. As a viscoelastic medium, the phase of the corresponding strain (φ_2) cannot be beyond that of the applied stress (φ_1). Therefore, the attenuations of elastic moduli are always nonnegative.

5.2. Relationship between Elastic Moduli Attenuation Inequality and Poisson's Ratio Attenuation. Using the definition of $1/Q = \mathrm{Imag(M)}/\mathrm{Real(M)}$ [23], we obtain the elastic moduli's attenuations, i.e., extensional attenuation $(1/Q_E)$, bulk attenuation $(1/Q_K)$, P-wave attenuation $(1/Q_P)$, and S-wave attenuation $(1/Q_S)$. The relationship between the

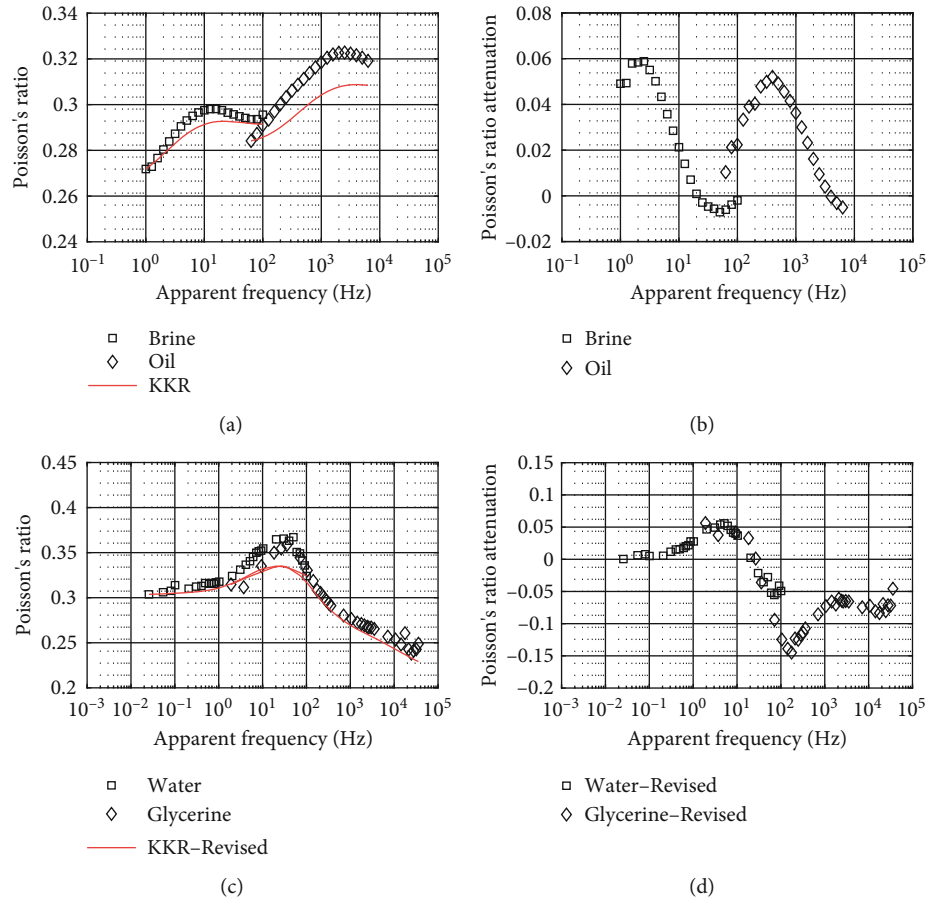

FIGURE 7: The frequency dependence of Poisson's ratio and it associated attenuation of fluid-saturated sandstone samples (from Sun et al. [17] and Pimienta et al. [20], respectively).

different attenuation modes is expressed in following [21]:

$$\begin{aligned}\frac{(1-\nu)(1-2\nu)}{Q_P} &= \frac{1+\nu}{Q_E} - \frac{2\nu(2-\nu)}{Q_S},\\ \frac{1-2\nu}{Q_K} &= \frac{3}{Q_E} - \frac{2(1+\nu)}{Q_S},\\ \frac{1+\nu}{Q_K} &= \frac{3(1-\nu)}{Q_P} - \frac{2(1-2\nu)}{Q_S}.\end{aligned} \tag{4}$$

Furthermore, the different attenuation modes are constrained to follow any one of three inequalities [21]:

$$\frac{1}{Q_K} > \frac{1}{Q_P} > \frac{1}{Q_E} > \frac{1}{Q_S}, \tag{5}$$

$$\frac{1}{Q_K} = \frac{1}{Q_P} = \frac{1}{Q_E} = \frac{1}{Q_S}, \tag{6}$$

$$\frac{1}{Q_K} < \frac{1}{Q_P} < \frac{1}{Q_E} < \frac{1}{Q_S}. \tag{7}$$

Rock physics scholars commonly hold that the inequality will change depending on the state of fluid saturation or the value of Poisson's ratio [38–40]. For the sandstones, the different attenuation modes mostly follow the first inequality (Equation (5)) for partial fluid saturation (small Poisson's ratio), while the different attenuation modes follow the third inequality (Equation (7)) for full fluid saturation (large Poisson's ratio) [38, 41]. However, for the carbonates, the different attenuation modes follow the first inequality (Equation (5)) for full fluid saturation (large Poisson's ratio) [39]. Here, we examine the relationship between the inequalities and fluid saturation state/Poisson's ratio using Poisson's ratio attenuation.

Gautam [38] rederived the attenuations $1/Q_S$, $1/Q_K$, and $1/Q_P$ using the attenuations $1/Q_E$, $1/Q_\nu$, and Poisson's ratio ν:

$$\frac{1}{Q_S} = \frac{1}{Q_E} - \frac{\nu}{1+\nu}\left(\frac{1}{Q_\nu}\right), \tag{8}$$

$$\frac{1}{Q_K} = \frac{1}{Q_E} + \frac{2\nu}{1-2\nu}\left(\frac{1}{Q_\nu}\right), \tag{9}$$

$$\frac{1}{Q_E} = \frac{1}{Q_E} + \frac{2(2-\nu)\nu^2}{(1-2\nu)(1-\nu^2)}\left(\frac{1}{Q_\nu}\right). \tag{10}$$

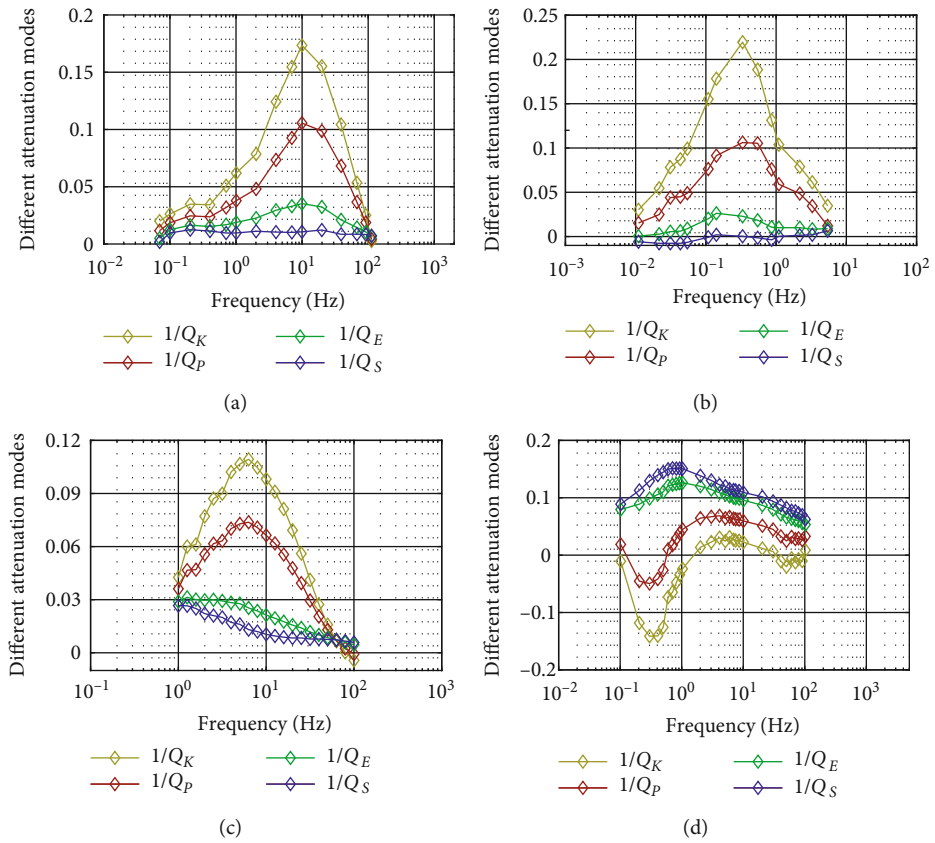

FIGURE 8: The relationship of different attenuation modes at different saturation state (from Sun et al. [18]; Borgomano et al. [15]; Sun et al. [17]; and Pimienta et al. [20],, respectively).

where the attenuation modes $1/Q_E$, $1/Q_S$, $1/Q_P$, $1/Q_K$, and Poisson's ratio ν (of sedimentary rocks) cannot be negative; the inequalities (i.e., Equations (5)–(7)) thus depend on the value of Poisson's ratio attenuation $1/Q_\nu$. If Poisson's ratio attenuation $1/Q_\nu$ is positive, with Equation (8), $1/Q_S$ is smaller than $1/Q_E$, and the different attenuation modes follow the first inequality (Equation (5)); if Poisson's ratio attenuation $1/Q_\nu$ is zero, $1/Q_S$ is equal to $1/Q_E$, and the different attenuation modes follow the second one (Equation (6)); and if Poisson's ratio attenuation $1/Q_\nu$ is negative, $1/Q_S$ is larger than $1/Q_E$, and the different attenuation modes follow the third one (Equation (7)). We conclude that the inequality between different attenuation modes does not depend on fluid saturation state (i.e., partial or full saturation) or Poisson's ratio but on Poisson's ratio attenuation. For partial saturation, when mesoscopic fluid flow mechanism dominates, Poisson ratio attenuation is positive (Sections 2.1 and 4.1), so the different attenuation modes always follow the first inequality (Equation (5)). For the transition from drained state to undrained state at full saturation and global fluid flow mechanism dominates, similar to partial saturation, Poisson ratio attenuation is also always positive (Sections 2.2.1 and 4.2) and the different attenuations follow the first inequality (Equation (5)). However, for the transition from undrained state to unrelaxed state at full saturation and squirt flow mechanism dominates, Poisson ratio attenuation can be positive or negative or zero, and the different attenuation modes can follow any one of the inequalities (i.e., Equations (5)–(7)), not just follow the third inequality (Equation (7)).

We compute the different attenuation modes corresponding to Figures 3–6 to show the effect of Poisson's ratio attenuation on the inequality which the different attenuation modes follow (Figure 8). Figure 8(a) corresponds to partial saturation in Figure 3. As Poisson's ratio attenuation is positive, the different attenuation modes follow the first inequality (Equation (5)). Similar to partial saturation, for the transition from drained state to undrained state at full saturation, the different attenuation modes follow the first inequality (Equation (5)) (Figure 8(b) corresponds to Figure 4). For the transition from undrained state to unrelaxed state at full saturation, when Poisson's ratio attenuation is positive, the different attenuation modes follow the first inequality (Equation (5)) (Figure 8(c) corresponds to Figure 5). On the other hand, when Poisson's ratio attenuation is negative, the different attenuation modes follow the third inequality (Equation (7)) (Figure 8(d) corresponds to Figure 6). The negative values of the attenuation modes can be attributed to the measurement error and the accumulation of attenuation calculation error.

6. Conclusion

In this paper, we investigated the frequency dependence of Poisson's ratio in fluid-saturated rock at both partial and full fluid saturation states. We theoretically summarized the frequency dependence of Poisson's ratio at different saturation states: (1) When rock is partially fluid-saturated or transits from drained state to undrained state at full fluid saturation, Poisson's ratio increases monotonously with frequency, and its attenuation is positive with one peak. (2) When rock transits from undrained state to unrelaxed state at full fluid saturation, three cases exist: 1) Poisson's ratio monotonously increases with frequency and has positive attenuation with one peak, 2) Poisson's ratio keeps constant with frequency and has zero attenuation, and 3) Poisson's ratio decreases monotonously with frequency and has negative attenuation with one peak. It is influenced by the concentrations of stiff and soft pores, the aspect ratio of soft pores, and the pore fluid bulk modulus. (3) When rock transits from drained state to unrelaxed state, the frequency-dependent Poisson's ratio can appear in two shapes: 1) step shape with two positive attenuation peaks and 2) bell shape with one positive attenuation peak and one negative attenuation peak.

A numerical modelling example was conducted to explore the effect of influence factors (the concentrations of stiff and soft pores, the aspect ratio of soft pores, and the pore fluid bulk modulus) on the frequency dependence of Poisson's ratio. It shows that the introduction of stiff and soft pores has a more important influence on the undrained Poisson's ratio than that at unrelaxed and dry states, but stiff pores and soft pores have opposite effect (decreasing or increasing). Then, the theoretical analysis of the frequency dependence of Poisson's ratio was validated by published data sets from literature, and the published data sets were verified by Kramers-Kronig relations.

Finally, based on the frequency dependence of Poisson's ratio attenuation, we reanalyzed and validated the relationship between different attenuation modes (i.e., $1/Q_K$, $1/Q_P$, $1/Q_E$, and $1/Q_S$). When Poisson's ratio attenuation is positive, different attenuation modes follow the inequality $1/Q_K > 1/Q_P > 1/Q_E > 1/Q_S$. When Poisson's ratio attenuation is 0, different attenuation modes follow the equality $1/Q_K = 1/Q_P = 1/Q_E = 1/Q_S$. When Poisson's ratio attenuation is negative, different attenuation modes follows the inequality $1/Q_K < 1/Q_P < 1/Q_E < 1/Q_S$. The relationship between different attenuation modes does not lie on saturation state (partial or full saturation) or Poisson's ratio but on Poisson's ratio attenuation. Once Poisson's ratio attenuation is obtained, the relationship between them can be easily determined.

These results help better understand the variation of Poisson's ratio (and different attenuation modes) at different frequencies and saturation states and can be used to improve the accuracy of geophysical data interpretation.

Appendix

A. CPEM Model

In the CPEM model, with noninteraction approximation, stiff and soft pores are simultaneously included into a solid mineral matrix. The elastic moduli are expressed explicitly [33]:

$$\frac{K_0}{K^C_{\text{sat-hf}}} = 1 + \phi_s \frac{3(1-\nu_0)}{2(1-2\nu_0)}\left(\frac{\delta_s}{1+\delta_s}\right) + \rho\frac{16\left(1-\nu_0^2\right)}{9(1-2\nu_0)}\left(\frac{\delta_c}{1+\delta_c}\right),$$
$$\frac{\mu_0}{\mu^C_{\text{sat-hf}}} = 1 + \phi_s \frac{15(1-\nu_0)}{7\text{-}5\nu_0} + \rho\left[\frac{16(1-\nu_0)}{15(1-(\nu_0/2))} + \frac{32(1-\nu_0)}{45}\left(\frac{\delta_c}{1+\delta_c}\right)\right], \tag{A.1}$$

where $K^C_{\text{sat-hf}}$ and $\mu^C_{\text{sat-hf}}$ are fluid-saturated bulk and shear moduli at unrelaxed state, respectively; K_0 and ν_0 are the bulk modulus and Poisson's ratio of the solid mineral matrix, respectively; ϕ_s is the stiff pore porosity; δ_s is the coupling parameter related to stiff pores; δ_c is the coupling parameter related to the soft pores; and ρ is the soft pore density. The coupling parameters δ_s, δ_c and the density ρ are obtained by

$$\delta_s = \frac{2E_0}{9(1-\nu_0)}\left(\frac{1}{K_f} - \frac{1}{K_0}\right), \tag{A.2}$$

$$\delta_c = \frac{\alpha\pi E_0}{4\left(1-\nu_0^2\right)}\left(\frac{1}{K_f} - \frac{1}{K_0}\right), \tag{A.3}$$

$$\phi_c = \frac{4}{3}\pi\alpha\rho, \tag{A.4}$$

where ϕ_c and α are the porosity and the aspect ratio of soft pores, respectively; E_0 is Young's modulus of the solid mineral matrix; and K_f is the pore fluid bulk modulus.

The dry/drained bulk and shear moduli (K^C_{dry} and μ^C_{dry}) for the rock is then obtained by taking the pore fluid bulk modulus as 0 in the coupling parameters δ_s, δ_c (i.e., Equations (A.2) and (A.3)):

$$\frac{K_0}{K^C_{\text{dry}}} = 1 + \phi_s \frac{3(1-\nu_0)}{2(1-2\nu_0)} + \rho\frac{16\left(1-\nu_0^2\right)}{9(1-2\nu_0)},$$
$$\frac{\mu_0}{\mu^C_{\text{dry}}} = 1 + \phi_s \frac{15(1-\nu_0)}{7\text{-}5\nu_0} + \rho\left[\frac{16(1-\nu_0)}{15(1-(\nu_0/2))} + \frac{32(1-\nu_0)}{45}\right]. \tag{A.5}$$

B. Zener Model

The viscoelastic Zener model is a combination of a spring in series with a parallel assemblage with a spring and a dashpot [20, 37]. In the model, the frequency-dependent modulus $M(\omega)$ and its attenuation $1/Q_M(\omega)$ are expressed as

$$M(\omega) = M_{\text{unrelaxed}} - \frac{M_{\text{unrelaxed}} - M_{\text{undrained}}}{1 + (\omega\tau)^2}, \tag{B.1}$$

$$1/Q_M(\omega) = \Delta M \frac{\omega\tau}{1 + (\omega\tau)^2}, \tag{B.2}$$

$$\Delta M = \frac{M_{\text{unrelaxed}} - M_{\text{undrained}}}{\sqrt{M_{\text{undrained}} M_{\text{unrelaxed}}}}, \tag{B.3}$$

where $M_{\text{unrelaxed}}$ is the unrelaxed modulus, $M_{\text{undrained}}$ is the undrained modulus, and τ is the relaxation time and obtained by $1/(2\pi f_0)$, and f_0 is the characteristic frequency where attenuation peak appears. The characteristic frequency f_0 is determined by [4]

$$f_0 = \frac{K_0 \alpha^3}{\eta}, \tag{B.4}$$

where K_0 is the bulk modulus of mineral matrix, α is the aspect ratio of soft pores in the rock, and η is the viscosity of pore fluid. The parameters have same definitions in the Numerical Modelling section.

Data Availability

Previously reported data were used to support this study and are available at [doi:10.1029/2021JB023867; doi:10.1002/2016JB013816; doi:10.1029/2020JB020132; doi:10.1190/GEO2015-0310.1]. These prior studies are cited at relevant places within the text as references [15, 17, 18, 20].

Conflicts of Interest

The authors declare that they have no conflicts of interest.

Acknowledgments

This research is supported by the National Key R&D Program of China [2021YFC2902003] and the National Natural Science Foundation of China [42104115, 42030810].

References

[1] N. I. Christensen, "Poisson's ratio and crustal seismology," *Journal of Geophysical Research*, vol. 101, no. B2, pp. 3139–3156, 1996.

[2] J. P. Dvorkin, "Can gas sand have a large Poisson's ratio," *Geophysics*, vol. 73, no. 2, pp. E51–E57, 2008.

[3] L. Zhou, J. Li, X. Chen, X. Liu, and L. Chen, "Prestack amplitude versus angle inversion for Young's modulus and Poisson's ratio based on the exact Zoeppritz equations," *Geophysical Prospecting*, vol. 65, no. 6, pp. 1462–1476, 2017.

[4] R. J. O'Connell and B. Budiansky, "Viscoelastic properties of fluid-saturated cracked solids," *Journal of Geophysical Research*, vol. 82, no. 36, pp. 5719–5735, 1977.

[5] G. Mavko and D. Jizba, "Estimating grain-scale fluid effects on velocity dispersion in rocks," *Geophysics*, vol. 56, no. 12, pp. 1940–1949, 1991.

[6] B. Gurevich, D. Makarynska, and M. Pervukhina, "Ultrasonic moduli for fluid-saturated rocks: Mavko-Jizba relations rederived and generalized," *Geophysics*, vol. 74, no. 4, pp. N25–N30, 2009.

[7] B. Gurevich, D. Makarynska, O. B. Paula, and M. Pervukhina, "A simple model for squirt-flow dispersion and attenuation in fluid-saturated granular rocks," *Geophysics*, vol. 75, no. 6, pp. N109–N120, 2010.

[8] J. Ba, J. Zhao, J. M. Carcione, and X. Huang, "Compressional wave dispersion due to rock matrix stiffening by clay squirt flow," *Geophysical Research Letters*, vol. 43, no. 12, pp. 6186–6195, 2016.

[9] M. L. Batzle, D. H. Han, and R. Hofmann, "Fluid mobility and frequency-dependent seismic velocity—direct measurements," *Geophysics*, vol. 71, no. 1, pp. N1–N9, 2006.

[10] N. Tisato and C. Madonna, "Attenuation at low seismic frequencies in partially saturated rocks: measurements and description of a new apparatus," *Journal of Applied Geophysics*, vol. 86, pp. 44–53, 2012.

[11] V. Mikhaltsevitch, M. Lebedev, and B. Gurevich, "A laboratory study of low-frequency wave dispersion and attenuation in water-saturated sandstones," *The Leading Edge*, vol. 33, no. 6, pp. 616–622, 2014.

[12] L. Pimienta, J. Fortin, and Y. Guéguen, "Bulk modulus dispersion and attenuation in sandstones," *Geophysics*, vol. 80, no. 2, pp. D111–D127, 2015.

[13] L. Pimienta, J. Fortin, and Y. Guéguen, "Experimental study of Young's modulus dispersion and attenuation in fully saturated sandstones," *Geophysics*, vol. 80, no. 5, pp. L57–L72, 2015.

[14] J. W. Spencer and J. Shine, "Seismic wave attenuation and modulus dispersion in sandstones," *Geophysics*, vol. 81, no. 3, pp. D211–D231, 2016.

[15] J. V. M. Borgomano, L. Pimienta, J. Fortin, and Y. Guéguen, "Dispersion and attenuation measurements of the elastic moduli of a dual-porosity limestone," *Journal of Geophysical Research: Solid Earth*, vol. 122, no. 4, pp. 2690–2711, 2017.

[16] H. Yin, J. Zhao, G. Tang, L. Zhao, X. Ma, and S. Wang, "Pressure and fluid effect on frequency-dependent elastic moduli in fully saturated tight sandstone," *Journal of Geophysical Research: Solid Earth*, vol. 122, no. 11, pp. 8925–8942, 2017.

[17] C. Sun, G. Tang, J. Fortin, J. V. M. Borgomano, and S. Wang, "Dispersion and attenuation of elastic wave velocities: Impact of microstructure heterogeneity and local measurements," *Journal of Geophysical Research: Solid Earth*, vol. 125, no. 12, article e2020JB020132, 2020.

[18] C. Sun, J. Fortin, J. V. M. Borgomano et al., "Influence of fluid distribution on seismic dispersion and attenuation in partially saturated limestone," *Journal of Geophysical Research: Solid Earth*, vol. 127, no. 5, article e2021JB023867, 2022.

[19] S. Chapman, J. V. M. Borgomano, B. Quintal, S. M. Benson, and J. Fortin, "Seismic wave attenuation and dispersion due to partial fluid saturation: Direct measurements and numerical simulations based on X-ray CT," *Journal of Geophysical Research: Solid Earth*, vol. 126, no. 4, article e2021JB021643, 2021.

[20] L. Pimienta, J. Fortin, and Y. Guéguen, "Effect of fluids and frequencies on Poisson's ratio of sandstone samples," *Geophysics*, vol. 81, no. 2, pp. D183–D195, 2016.

[21] K. Winkler and A. Nur, "Pore fluids and seismic attenuation in rocks," *Geophysical Research Letters*, vol. 6, no. 1, pp. 1–4, 1979.

[22] H. Gercek, "Poisson's ratio values for rocks," *International Journal of Rock Mechanics & Mining Sciences*, vol. 44, no. 1, pp. 1–13, 2007.

[23] R. J. O'Connell and B. Budiansky, "Measures of dissipation in viscoelastic media," *Geophysical Research Letter*, vol. 5, no. 1, pp. 5–8, 1978.

[24] G. Mavko, T. Mukerji, and J. Dvorkin, *The rock physics handbook: Tools for seismic analysis of porous media*, p. 18, Cambridge University Press, 1998.

[25] J. E. White, "Computed seismic speeds and attenuation in rocks with partial gas saturation," *Geophysics*, vol. 40, no. 2, pp. 224–232, 1975.

[26] V. Mikhaltsevitch, M. Lebedev, and B. Gurevich, "Validation of the laboratory measurements at seismic frequencies using the Kramers-Kronig relationship," *Geophysical Research Letter*, vol. 43, no. 10, pp. 4986–4991, 2016.

[27] N. C. Dutta and H. Odé, "Attenuation and dispersion of compressional waves in fluid-filled porous rocks with partial gas saturation (white model)—part I: biot theory," *Geophysics*, vol. 44, no. 11, pp. 1777–1788, 1979.

[28] N. C. Dutta and A. J. Seriff, "On White's model of attenuation in rocks with partial gas saturation," *Geophysics*, vol. 44, no. 11, pp. 1806–1812, 1979.

[29] L. Pimienta, J. V. M. Borgomano, J. Fortin, and Y. Guéguen, "Modelling the drained/undrained transition: effect of the measuring method and the boundary conditions," *Geophysical Prospecting*, vol. 64, no. 4, pp. 1098–1111, 2016.

[30] C. Sun, G. Tang, J. Zhao et al., "Three-dimensional numerical modelling of the drained/undrained transition for frequency-dependent elastic moduli and attenuation," *Geophysical Journal Internaitonal*, vol. 219, no. 1, pp. 27–38, 2019.

[31] V. Mikhaltsevitch, M. Lebedev, R. Chavez, M. Pervukhina, S. Glubokovskikh, and E. Vargas Jr., "The dead volume effect on the elastic moduli measurements using the forced-oscillation method," *Geophysical Prospecting*, vol. 70, no. 3, pp. 547–557, 2022.

[32] A. Endres and R. Knight, "Incorporating pore geometry and fluid pressure communication into modeling the elastic behavior of porous rocks," *Geophysics*, vol. 62, no. 1, pp. 106–117, 1997.

[33] M. Adelinet, J. Fortin, and Y. Guéguen, "Dispersion of elastic moduli in a porous-cracked rock: theoretical predictions for squirt-flow," *Tectonophysics*, vol. 503, no. 1-2, pp. 173–181, 2011.

[34] M. Le Ravalec, Y. Guéguen, and T. Chelidze, "Elastic wave velocities in partially saturated rocks: saturation hysteresis," *Journal of Geophysical Research-Solid Earth*, vol. 101, no. B1, pp. 837–844, 1996.

[35] L. Zhao, T. Chen, T. Mukerji, and G. Tang, "Bulk modulus for fluid-saturated rocks at high frequency: modification of squirt flow model proposed by Mavko and Jizba," *Geophysical Journal International*, vol. 225, no. 3, pp. 1714–1724, 2021.

[36] T. D. Jones, "Pore fluids and frequency-dependent wave propagation in rocks," *Geophysics*, vol. 51, no. 10, pp. 1939–1953, 1986.

[37] G. Mavko, T. Mukerji, and J. Dvorkin, *The rock physics handbook: tools for seismic analysis of porous media*, p. 71, Cambridge University Press, 1998.

[38] K. Gautam, *Fluid effects on attenuation and dispersion of elastic waves*, University of Colorado, 2003.

[39] L. Adam, M. Batzle, K. T. Lewallen, and K. Wijk, "Seismic wave attenuation in carbonates," *Journal of Geophysical Research*, vol. 114, no. B6, pp. B06208–B06221, 2009.

[40] M. L. Batzle, K. Gautam, R. Hofmann, L. Duranti, and L. Adam, "Seismic-frequency loss mechanisms: direct observation," *The Leading Edge*, vol. 33, no. 6, pp. 656–662, 2014.

[41] K. Winkler and A. Nur, "Seismic attenuation: effects of pore fluids and frictional-sliding," *Geophysics*, vol. 47, no. 1, pp. 1–15, 1982.